



This discussion paper is/has been under review for the journal Atmospheric Chemistry and Physics (ACP). Please refer to the corresponding final paper in ACP if available.

A parameterization of sub-grid particle formation in sulphur-rich plumes for global and regional-scale models

R. G. Stevens¹ and J. R. Pierce^{1,2}

¹Department of Physics and Atmospheric Science, Dalhousie University, Halifax, NS, Canada

²Department of Atmospheric Science, Colorado State University, Fort Collins, CO, USA

Received: 10 July 2013 – Accepted: 15 July 2013 – Published: 25 July 2013

Correspondence to: R. G. Stevens (rgstevens@dal.ca)

Published by Copernicus Publications on behalf of the European Geosciences Union.

A parameterization of sub-grid particle formation

R. G. Stevens and
J. R. Pierce

Title Page

Abstract

Introduction

Conclusions

References

Tables

Figures



Back

Close

Full Screen / Esc

Printer-friendly Version

Interactive Discussion

Abstract

New-particle formation in the plumes of coal-fired power plants and other anthropogenic sulphur sources may be an important source of particles in the atmosphere. It remains unclear, however, how best to reproduce this formation in global and regional aerosol models with grid-box lengths that are tens of kilometres and larger. Based on the results of the System for Atmospheric Modelling (SAM), a Large-Eddy Simulation/Cloud-Resolving Model (LES/CRM) with online Two Moment Aerosol Sectional (TOMAS) microphysics, we have developed a computationally efficient, but physically based, parameterization that predicts the characteristics of aerosol formed within sulphur-rich plumes based on parameters commonly available in global- and regional-scale models. Given large-scale mean meteorological parameters ((1) wind speed, (2) boundary-layer height and (3) downward shortwave radiative flux), (4) emissions of SO₂ and (5) NO_x from the source, (6) mean background condensation sink, (7) background SO₂ and (8) NO_x concentrations, and (9) the desired distance from the source; the parameterization will predict: (1) the fraction of the emitted SO₂ that is oxidized to H₂SO₄, (2) the fraction of that H₂SO₄ that forms new particles instead of condensing onto preexisting particles, (3) the mean mass per particle of the newly formed particles, and (4) the number of newly formed particles per kilogram SO₂ emitted. The parameterization we describe here should allow for more accurate predictions of aerosol size distributions and a greater confidence in the effects of aerosols in climate and health studies.

1 Introduction

It is well known that the size of atmospheric aerosols strongly impacts the magnitude of their direct radiative effect (Charlson et al., 1992) and their ability to act as cloud condensation nuclei (CCN) (Dusek et al., 2006), thereby increasing cloud reflectivity and lifetime (Albrecht, 1989; Twomey, 1974). The uncertainty in the effects of aerosols

ACPD

13, 19583–19623, 2013

A parameterization of sub-grid particle formation

R. G. Stevens and
J. R. Pierce

Title Page

Abstract

Introduction

Conclusions

References

Tables

Figures

⏪

⏩

◀

▶

Back

Close

Full Screen / Esc

Printer-friendly Version

Interactive Discussion

A parameterization of sub-grid particle formation

R. G. Stevens and
J. R. Pierce

Title Page

Abstract

Introduction

Conclusions

References

Tables

Figures

⏪

⏩

◀

▶

Back

Close

Full Screen / Esc

Printer-friendly Version

Interactive Discussion

dominates the uncertainty in radiative forcing changes (Forster et al., 2007). These aerosols are also known to cause respiratory problems in humans (Dockery et al., 1993), and those particles smaller than 100 nm in diameter may have greater health impacts than larger particles (Peters et al., 1997). Thus, it is important to understand aerosol number and size for both climate and health.

One of the largest anthropogenic sources of aerosol mass are sulphur-rich plumes (Dentener et al., 2006). Sulphur dioxide (SO_2) within these plumes can be oxidized by the hydroxyl radical (OH) to form sulphuric acid (H_2SO_4), which in turn can condense onto pre-existing particles. If H_2SO_4 concentrations are high enough, the H_2SO_4 will cluster with itself and other condensable gases to nucleate new particles (Kulmala and Kerminen, 2008). This anthropogenic sulphur has a significant effect on particle concentrations globally, particularly in the Northern Hemisphere (Adams and Seinfeld, 2003; Luo and Yu, 2011; Spracklen et al., 2005; Wang and Penner, 2009).

However, the concentrations of OH are sensitive to NO_x (nitric oxide, (NO) + nitrogen dioxide, (NO_2) concentrations, which will vary across a given plume (Lonsdale et al., 2012). Together with the heterogeneity of the condensation sink (approximately proportional to aerosol surface area) within a plume, this causes the H_2SO_4 concentrations to vary dramatically within a plume. Nucleation and growth rates, which are strong functions of H_2SO_4 concentrations, will in turn vary spatially across a plume. Finally, the coagulation sink of these newly formed particles will also be location-dependant in these plumes, which typically have widths of up to tens of kilometres during the first several hundred kilometres of movement. Currently, global- and regional-scale models typically have resolutions of hundreds and tens of kilometres or more, respectively, and are thus unable to accurately resolve the formation and growth of aerosols within these plumes using grid-box averages for chemical concentrations, aerosol concentrations, and meteorological values.

Therefore, these models have typically assumed that some fraction of all anthropogenic SO_2 emissions are oxidized to form sulphate (SO_4) at the sub-grid scale using a single size distribution for all anthropogenic sulphate sources. For instance, the study

A parameterization of sub-grid particle formation

R. G. Stevens and
J. R. Pierce

Title Page

Abstract

Introduction

Conclusions

References

Tables

Figures



Back

Close

Full Screen / Esc

Printer-friendly Version

Interactive Discussion

of Makkonen et al. (2009) used the assumption recommended by the AeroCom emissions inventory (Dentener et al., 2006): the sulphate was emitted into a single lognormal mode with a median radius of 500 nm and a standard deviation of 2.0. A number of studies (Adams and Seinfeld, 2002, 2003; Pierce and Adams, 2006, 2009; Pierce et al., 2007; Spracklen et al., 2005) have used a bi-modal distribution comprised of a nucleation mode and an accumulation mode with number mean diameters 10 nm and 70 nm, and geometric standard deviations 1.6 and 2.0. Either 5 % or 15 % of the sulphate mass is emitted into the nucleation mode, depending on the study. Yet another approach was used in the study of Yu and Luo (2009), they emitted 5 % of sulphur mass into the aforementioned nucleation mode and condensed the remaining mass onto the existing accumulation-mode particles. As some of the sulphate formed in the plume must condense onto the preexisting particles that have been entrained into the plume, this approach is, in this way, more realistic than the other assumptions.

While the studies listed above differ in the amount and size of sub-grid sulphate particles, they all assume that these values are constant regardless of the meteorological and chemical characteristics of the emissions plumes. However, several studies have shown that the particle formation in plumes is strongly sensitive to environmental conditions. Yu (2010) showed that differences in temperature and hydroxyl concentrations cause the size and number of aerosol particles to vary seasonally and diurnally. Lonsdale et al. (2012) showed that the number of particles formed within sulphur-rich plumes is strongly dependent on the emission rates of both SO₂ and NO_x from the source. In addition, we have shown in Stevens et al. (2012) that the background aerosol concentrations and the meteorology have strong effects on number and size of aerosol formed within such plumes. However, there is currently no means of representing these dependencies of plume-scale particle formation in global and regional models.

Several global studies have already investigated the sensitivity of global CCN concentrations to the assumptions made regarding sub-grid sulphate formation. Luo and Yu (2011) varied the fraction of emitted sulphate that was emitted into the nucleation mode from 5 % to 15 %, and found that this increased the CCN at an assumed super-

A parameterization of sub-grid particle formation

R. G. Stevens and
J. R. Pierce

Title Page

Abstract

Introduction

Conclusions

References

Tables

Figures

⏪

⏩

◀

▶

Back

Close

Full Screen / Esc

Printer-friendly Version

Interactive Discussion

saturation of 0.2 % (CCN(0.2 %)) by up to 18 % over source regions. Furthermore, they found that changing the fraction of emitted SO₂ converted to sub-grid sulphate from 0 % to 5 % changed global boundary-layer CCN(0.2 %) by 11 %. The earlier studies of Adams and Seinfeld (2003) and Spracklen et al. (2005) used the 10- and 70-nm mode sub-grid sulfate assumptions described above. Each found that if the fraction of SO₂ converted to sub-grid sulphate was changed from 0 % to 3 %, CCN(0.2 %) in polluted areas would double. Adams and Seinfeld (2003) included only sulphate aerosol in their model, and Spracklen et al. (2005) included only sulphate and sea-salt aerosol, so this was believed to be an upper limit for this effect. However, the study of Wang and Perner (2009), which included organic matter, black carbon, and dust, varied the fraction of SO₂ converted to sub-grid sulphate over a smaller range (0 % to 2 %), and also found that CCN(0.2 %) more than doubled over polluted areas. Additionally, they found that CCN(0.2 %) increased by 23 % to 53 % averaged over global boundary layer, and that the aerosol indirect effect radiative forcing increased by 11 % to 31 % (depending on the grid-resolved nucleation scheme used in the boundary layer). CCN concentrations and regional radiative forcings are thus clearly sensitive to the assumptions regarding sulphur partitioning and the size of aerosol formed in sulphur-rich plumes.

Lee et al. (2013) recently quantified the uncertainty in CCN concentrations that was due to 28 different uncertain inputs in the GLOMAP global aerosol model. Based on the results of Stevens et al. (2012), the range of possible values for the diameter of sub-grid sulphate particles used in Lee et al. (2013) was reduced to a smaller range than the full range of sub-grid-sulphate assumptions used previously in studies, which lead to a reduced estimation of the uncertainty in CCN concentrations attributable to this input compared to the range of estimates described in the previous paragraph. Even with the reduced ranges, the uncertainties in sub-grid SO₄ production was found to be just as important as the uncertainties in SO₂ emission rates, and had the largest contribution of the 28 inputs to the uncertainty in CCN concentrations over polluted North America and Europe. Globally, the uncertainty in sub-grid-sulphate particle size ranked as the twelfth largest contributor to the relative uncertainties in CCN concentrations of the 28

inputs tested. These large uncertainties in CCN prediction due to sub-grid sulfate formation highlight the need for improved representation of plume-scale particle formation in global and regional models.

In this paper, we develop a computationally efficient, but physically based, parameterization that predicts the characteristics of aerosol formed within sulphur-rich plumes based on parameters commonly available in global- and regional-scale models. This parameterization is based on the results of the System for Atmospheric Modelling (SAM) (Khairoutdinov and Randall, 2003), a Large-Eddy Simulation/Cloud-Resolving Model (LES/CRM) with online Two-Moment Aerosol Sectional (TOMAS) microphysics (Adams and Seinfeld, 2002) that has been tested against aircraft observations of particle formation in plumes (Lonsdale et al., 2012; Stevens et al., 2012). Given large-scale mean meteorological parameters (1) wind speed, v_g , (2) boundary layer height, BLH, and (3) downward shortwave radiative flux, DSWRF, (4) emissions of SO_2 , SO_2emis , and (5) NO_x , NO_xemis , from the source, (6) mean background condensation sink, CS, (7) mean background SO_2 , bgSO_2 , and (8) NO_x , bgNO_x , concentrations, and (9) the desired distance from the source, d , the Predicting Particle Production in Power-Plant Plumes (P6) parameterization predicts (1) the fraction of the emitted SO_2 that is oxidized to form H_2SO_4 , f_{ox} , (2) the fraction of that H_2SO_4 that forms new particles instead of condensing onto preexisting particles, f_{new} , (3) the mean mass per particle of the newly formed particles, M_m , and (4) the number of newly formed particles per mass of SO_2 emitted, N_{new} .

In Sect. 2 we provide a brief description of the SAM-TOMAS model and how the P6 training data was selected. Section 3 describes the form and physical basis of the P6 parameterization. The evaluation of the P6 parameterization against the full SAM-TOMAS model is presented in Sect. 4. We describe sensitivity studies performed using the parameterization in Sect. 5. Finally, we present our conclusions in Sect. 6.

A parameterization of sub-grid particle formation

R. G. Stevens and
J. R. Pierce

Title Page

Abstract

Introduction

Conclusions

References

Tables

Figures

⏪

⏩

◀

▶

Back

Close

Full Screen / Esc

Printer-friendly Version

Interactive Discussion

2 Description of SAM-TOMAS model and training data

A full description of the SAM-TOMAS model is available in Stevens et al. (2012), so we will restrict ourselves to a brief summary here. The SAM model (Khairoutdinov and Randall, 2003) is a flexible LES/CRM model with a resolution of tens of metres to several kilometres, and a domain that can span tens to thousands of kilometres. The TOMAS microphysics algorithm (Adams and Seinfeld, 2002; Pierce and Adams, 2009) in SAM resolves aerosol by both mass and number independently in 15 size bins spanning 3 nm to 10 μm . Condensation, coagulation, and nucleation are explicitly resolved in the model. Sulphate, ammonium (NH_3), aerosol water, and the gas-phase concentrations of SO_2 , NO_x , ammonia (NH_4) and H_2SO_4 are simulated within the model, but secondary organic aerosol formation is not explicitly simulated under the assumption that sulphate aerosol formation will dominate within sulphur-rich plumes.

The concentration of OH in the SAM-TOMAS model is currently parametrized based off of the downward shortwave radiative flux (DSWRF) and the concentration of NO_x . This OH parameterization is an empirical fit to results from the detailed time-dependent photochemical box model described by Olson et al. (2006). However, the uncertainties associated with the parametrized OH become large for solar zenith angles larger than 70° , which, for clear-sky conditions, correspond to DSWRF values less than 350 W m^{-2} . In addition, we do not account for nitrous acid (HONO) or sulphur trioxide (SO_3) emission, which may account for additional sulphuric acid formation. Both of these emissions may result in particle formation early in the plume, and may account for the under-prediction of particles within 5 km of the stack in Stevens et al. (2012). However, we note that these processes do not seem to be necessary to accurately predict particle size and number concentrations beyond 30 km from the source. When these processes become better understood, we plan to incorporate them into a future version of the P6 parameterization.

During cloudy conditions, SO_2 may undergo aqueous oxidation through reaction with H_2O_2 or other species (Zhou et al., 2012). Currently, this is not accounted for in the

ACPD

13, 19583–19623, 2013

A parameterization of sub-grid particle formation

R. G. Stevens and
J. R. Pierce

Title Page

Abstract

Introduction

Conclusions

References

Tables

Figures

⏪

⏩

◀

▶

Back

Close

Full Screen / Esc

Printer-friendly Version

Interactive Discussion

A parameterization of sub-grid particle formation

R. G. Stevens and
J. R. Pierce

Title Page

Abstract

Introduction

Conclusions

References

Tables

Figures

⏪

⏩

◀

▶

Back

Close

Full Screen / Esc

Printer-friendly Version

Interactive Discussion

SAM-TOMAS model. Therefore, SO₂ oxidation is likely underestimated under cloudy conditions. Under such conditions, however, less new-particle formation is expected because DSWRF, and subsequently oxidation of SO₂ though reaction with OH will also be suppressed. Also, the additional surface area from cloud droplets in the clouds and cloud-processed aerosols outside of the clouds will slow nucleation and increase coagulative losses of new particles. We therefore do not believe that this would be a significant uncertainty for predicting the number and size of aerosol formed in sulphur-rich plumes.

For this study, the model was operated as a Lagrangian 2-D wall model that passed over the power-plant after a spin-up period of 1800 s of model time. The wall extends upwards and horizontally perpendicular to the direction of the mean boundary-layer wind. We have evaluated the model operating in Lagrangian mode against the Eulerian mode used in Stevens et al. (2012), and we have found that the discrepancies in NO_x and SO₂ concentrations between the two models are less than one standard deviation of the concentrations (due to variability in time). Similarly, the total particle concentration within the plume differed by less than 16 % between the Lagrangian and the Eulerian modes, and the particle size distributions had similar characteristics in both models. Both models compare similarly well to the measurements shown in Stevens et al. (2012).

In the simulations used here, the model resolution was held fixed at 400 m × 400 m × 40 m and the model domain was 120 km wide and 5 km high. We chose an empirical activation-type nucleation scheme (Kulmala et al., 2006), where nucleation rates are calculated as 10⁻⁷ s⁻¹ · [H₂SO₄], because this scheme provided the best match to observations out of the 6 schemes tested in Stevens et al. (2012).

In order to determine the best-fit parameters for the P6 parameterization, we performed many simulations using the SAM-TOMAS model using a realistic range of different inputs for the emissions, meteorology, and background aerosol and trace gas concentrations. In order to choose realistic, but sufficiently diverse, conditions for the simulations, we performed the procedure described in the following three paragraphs.

A parameterization of sub-grid particle formation

R. G. Stevens and
J. R. Pierce

Title Page

Abstract

Introduction

Conclusions

References

Tables

Figures

⏪

⏩

◀

▶

Back

Close

Full Screen / Esc

Printer-friendly Version

Interactive Discussion

To generate a data set of realistic aerosol size distributions and trace gas concentrations, we used output from the GEOS-Chem-TOMAS model. GEOS-Chem-TOMAS uses the TOMAS aerosol microphysics module described above in the GEOS-Chem chemical transport model (www.geos-chem.org, Bey et al., 2001). The implementation of TOMAS in GEOS-Chem has been discussed previously (Pierce et al., 2013; Snow-Kropla et al., 2011; Trivitayanurak et al., 2008). Variables were output every 3 h. The model resolution was $0.5^\circ \times 0.666^\circ$. We used Latin Hypercube sampling (a method of pseudo-randomly choosing a set of samples from a multi-dimensional space such that the full range of each dimension is sampled, but the coordinates in each dimension are uncorrelated) to determine a set of 5000 (1) latitudes, (2) longitudes, (3) date and time, (4) distances from the emissions source (d), (5) emissions rate of SO_2 (SO_2emis) and (6) NO_x (NO_xemis), and (7) the effective emissions height, which implicitly includes both the height of the emissions stack and the initial buoyant rise of the plume. The range of values used for each of these variables is listed in Table 1. We note that while only the month of July was sampled to create the training data, the large geographic range used provided diverse meteorological conditions. As the OH parameterization used in the SAM-TOMAS model has high uncertainties for large solar zenith angles, we excluded from our range of times to be selected the hours of 03:00, 06:00, and 09:00 UTC as these should be at high solar zenith angles or outside daylight hours for the latitude and longitude range we selected. In order to further reduce the number of cases with high solar zenith angles, we subsequently excluded from our analysis any cases that had DSWRF values less than 100 W m^{-2} . We then obtained the background aerosol size distribution, background SO_2 and NO_x concentrations (bgSO_2 and bgNO_x), and DSWRF from the GEOS-Chem-TOMAS output that corresponded to each set of latitude, longitude, date and time. The maximum, minimum, and median values of these outputs from GEOS-Chem-TOMAS are shown in Table 2.

To drive the dynamics in SAM-TOMAS, we obtained for each set of latitude, longitude, date, and time the corresponding profiles of potential temperature, water vapour mixing ratio, wind speed and direction; surface fluxes of sensible heat, latent heat,

A parameterization of sub-grid particle formation

R. G. Stevens and
J. R. Pierce

Title Page

Abstract

Introduction

Conclusions

References

Tables

Figures

⏪

⏩

◀

▶

Back

Close

Full Screen / Esc

Printer-friendly Version

Interactive Discussion

and momentum; the boundary-layer height (BLH) and the surface pressure from the National Center for Environmental Prediction (NCEP) North American Regional Reanalysis (NARR) (Mesinger et al., 2006) assimilated meteorology data, as was done for the study of Stevens et al., (2012). The reanalysis data were provided by the National Oceanic and Atmospheric Administration (NOAA), Ocean and Atmospheric Research (OAR), Earth System Research Laboratory (ESRL) Physical Sciences Division (PSD), Boulder, Colorado, USA, from their website at: <http://www.esrl.noaa.gov/psd/>. The NCEP NARR data was chosen for this study because the software necessary to create input files from reanalysis data was readily available. We note that while the meteorology from the reanalysis data may not correspond exactly to the data from the GEOS-Chem-TOMAS model due to differences in spatial and temporal resolution, an exact match is not necessary to create a realistic set of training inputs.

For each simulation using the SAM-TOMAS model, we used SO_2 emis, NO_x emis and effective emissions height from the Latin hypercube sample; the background aerosol size distribution, bgSO_2 , bgNO_x , and DSWRF from the output of the GEOS-Chem-TOMAS model; and the SAM-TOMAS meteorology that was driven by nudging and boundary conditions from the NCEP-NARR assimilated meteorology data. We ran the model until the emissions reached the distance from the source specified from the Latin hypercube sample. We preserved the following variables as training inputs for the P6 parameterization: (1) SO_2 emis, (2) NO_x emis, (3) total condensation sink of the background aerosol size distribution (CS), (4) DSWRF, (5) the mean wind speed within the boundary layer (v_g), (6) BLH, (7) the distance from the source (d), (8) bgSO_2 , and (9) bgNO_x . The maximum and minimum values of these parameters are shown in Tables 1, 2, and 3. Other information necessary to run the SAM-TOMAS model, such as the effective emissions height, the potential temperature profile, the water vapour mixing ratio profile, and the surface fluxes may not be available in many regional- and global-scale models and the current P6 inputs capture most of the variability in aerosol formation and growth within plumes, as we will show in Sect. 5. We have therefore excluded them as inputs to the parameterization. However, by including a wide range

A parameterization of sub-grid particle formation

R. G. Stevens and
J. R. Pierce

Title Page

Abstract

Introduction

Conclusions

References

Tables

Figures

⏪

⏩

◀

▶

Back

Close

Full Screen / Esc

Printer-friendly Version

Interactive Discussion

of high-emitters, medium-emitters, and low-emitters. We define high-emitters, medium-emitters, and low-emitters based on the emissions data for power-plants in the United States compiled from the Clean Air Markets (CAM) data (United States Environmental Protection Agency, 2012) as follows: for medium-emitters, we use the log-space mean emission rates for a power plant in the USA during 2010. For low and high emitters, we use an emission rate that is one standard deviation below or above the mean in log space, respectively. The high, median, and low emissions rates are listed in Table 4. (3) If the SO_2 emissions are known, but the NO_x emissions are not known (or the NO_x emissions from the major SO_2 sources are not known), the median $\text{SO}_2 : \text{NO}_x$ emissions ratio of 0.419 from the 2010 EPA CAM data will be assumed (as well as the high-, medium- and low-emitter assumptions from the previous P6 mode).

Even if the precise locations of power plants are known, it may not be clear at what distance from the source the particles are well-mixed within a grid box that also contains the source of emissions. However, as we will show in Sect. 5, the P6 values of M_m , N_{new} , and f_{new} are not strongly sensitive to the distance from the source beyond distances of 30 km, and f_{ox} depends less than linearly on the distance from the source.

In the following subsections, we describe the theory and semi-empirical fits behind the P6 parameterization.

3.1 Fraction oxidized

In order to formulate a semi-empirical equation for f_{ox} , we first formulate a semi-empirical equation for the effective NO_x mixing ratio within the plume because NO_x modulates the OH concentrations and thus affects the oxidation rate of SO_2 . The mean concentration of NO_x within the plume should be equal to the sum of the contributions from the background and the emitted NO_x after accounting for dilution, which should be related to v_g , BLH, and the time since emission, calculated as (d/v_g) . We therefore

calculate the effective NO_x concentration, NO_{x,eff}, as:

$$\text{NO}_{x,\text{eff}} = \text{bgNO}_x + 1.444 \times 10^{-8} \frac{\text{NO}_{x,\text{emis}}}{v_g^{1.234} \text{BLH}^{0.2018} \left(\frac{d}{v_g}\right)^{0.7902}} \quad (1)$$

where the exponents for v_g , BLH, and (d/v_g) have been fit for this equation to the average concentrations of NO_x in the plume using the training data (evaluation of the fit in Sect. 4). We allowed the scaling factor of 1.444×10^{-8} to be freely fit to the data, because the relative importance of the background concentrations and the emitted NO_x is different for the f_{ox} than it is for the mean concentration of NO_x. As the relative importance of background and emitted NO_x is also different for determining nucleation, M_m , and N_{new} , we list the scaling factors used to calculate NO_{x,eff} for each of these outputs in Table 5. The scaling factor found when fitting to the mean NO_x concentration within the plume was 9.595×10^4 . However, the best fit scaling factor found for calculating f_{ox} is much lower, such that the NO_{x,eff} is dominated by bgNO_x. Generally, NO_x concentrations are sufficiently high within the centre of the plume (and early in the plume) to prevent fast oxidation of SO₂, so the background concentrations are relatively much more important to f_{ox} than they are to the mean NO_x concentration within the plume.

We calculate an effective OH concentration using the same parameterization that is used in the SAM-TOMAS model. This parameterization calculates the OH concentration as a function of the NO_x concentration within the plume and the DSWRF. The parameterization, which is a fit of chemistry box-model simulations of Olson et al. (2006), was originally described in Appendix A of Stevens et al., (2012).

First, we set variables x and y :

$$x = \log(\text{NO}_{x,\text{eff}}) - 0.195 \quad (2)$$

$$y = \frac{\text{DSWRF}}{S_0 \cdot T} \quad (3)$$

A parameterization of sub-grid particle formation

R. G. Stevens and
J. R. Pierce

Title Page

Abstract

Introduction

Conclusions

References

Tables

Figures

⏪

⏩

◀

▶

Back

Close

Full Screen / Esc

Printer-friendly Version

Interactive Discussion



where S_0 is the solar constant at the top of the atmosphere, 1370 W m^{-2} , and T is an assumed transmittance of the clear atmosphere, 0.76. We then calculate two polynomials, the first (P1) estimating the shape of the OH vs. NO_x relationship, and the second (P2) capturing the dependence of OH on DSWRF:

$$P1 = -0.014x^6 + 0.0027x^5 + 0.1713x^4 - 0.0466x^3 - 0.7893x^2 - 0.1739x + 6.9414 \quad (4)$$

$$P2 = (-1345y^3 + 4002y^2 - 471.8y + 42.72) \cdot 10^4 \quad (5)$$

From P1 and P2, we calculate the effective OH concentration, OH_{eff} :

$$[\text{OH}] = 0.82 \cdot 10^{\text{P1} \cdot \log(\text{P2}) / 6.8} \quad (6)$$

If we assume that the only loss mechanism for SO_2 is through reaction with OH (e.g. clear skies and ignore reactions with Criegee intermediates, Mauldin et al., 2012), and we knew the true OH concentrations, we could calculate f_{ox} by using the rate constant k , the time elapsed t and the following equation:

$$f_{\text{ox}} = 1 - \exp(-k[\text{OH}]t) \quad (7)$$

However, given that OH_{eff} is not the true concentration, and we must calculate t as d/v_g , we use the analogous equation:

$$f_{\text{ox}} = 1 - \exp\left(-1.650 \times 10^{-10} \text{OH}_{\text{eff}}^{0.7904} \left(\frac{d}{v_g}\right)^{0.7723}\right) \quad (8)$$

where the numerical values have been selected by minimizing the error between the P6 fit f_{ox} values and the predicted f_{ox} from the SAM-TOMAS simulations. As the best-fit $\text{NO}_{x,\text{emis}}$ scaling factor for calculation of $\text{NO}_{x,\text{eff}}$ is near zero, OH_{eff} is approximately equal to the OH concentration outside of the plume in the f_{ox} calculation. Since NO_x concentrations will generally be sufficiently high within the plume that OH within the plume is less than at the plume edges, the best fit exponent for OH_{eff} is less than one. Oxidation of SO_2 subsequently proceeds more slowly within the plume than at the edges, thus the best-fit exponent for (d/v_g) is also less than one.

A parameterization of sub-grid particle formation

R. G. Stevens and
J. R. Pierce

Title Page

Abstract

Introduction

Conclusions

References

Tables

Figures

⏪

⏩

◀

▶

Back

Close

Full Screen / Esc

Printer-friendly Version

Interactive Discussion



3.3 Mean mass per particle of new particles

If we predict that there will be significant nucleation, we then predict the mean mass per particle of the newly formed particles. We expect that the particles will be growing primarily through condensation of available H_2SO_4 . Therefore, we expect that the mean mass per particle, M_m , will be proportional to the product of the time elapsed (d/v_g), f_{ox} and $\text{SO}_{2,\text{eff}}$. Since the pre-existing particles will be competing for the available H_2SO_4 , we divide this value by the background condensation sink, CS, the first-order rate constant of the loss of condensable vapor by condensation, which is proportional to the Fuchs-corrected surface area of the particles (Kerminen et al., 2004). We add a constant minimum value to this, which corresponds to the smallest size of aerosol that can be resolved by the SAM-TOMAS model. In this way we arrive at the following equation for M_m :

$$M_m = 1.475 \times 10^{-27} \frac{f_{\text{ox}}^{1.517} \text{SO}_{2,\text{eff}}^{1.094}}{\text{CS}^{0.6173}} \left(\frac{d}{v_g} \right)^{0.9685} + 4.071 \times 10^{-23} \text{ kg} \quad (11)$$

Again, we include the fitted parameters in this equation, and the fit will be evaluated in Sect. 4.

However, we note that the free parameters for predicting f_{ox} were optimized to reduce the rms absolute error between the parametrized f_{ox} and the SAM-TOMAS predicted f_{ox} to a minimum, and we are more interested in minimizing the rms relative error in M_m , since M_m spans several orders of magnitude. We therefore allowed the free parameters used to predict f_{ox} to change when we sought the parameters that minimize the root-mean-square error in $\log_{10}(M_m)$. Notably, the NO_x emis scaling factor (Eq. 1) used within the calculation of M_m is several orders of magnitude larger than that used within the calculation of f_{ox} , as listed in Table 5. We will discuss this difference further in Sect. 5.

A parameterization of sub-grid particle formation

R. G. Stevens and
J. R. Pierce

[Title Page](#)[Abstract](#)[Introduction](#)[Conclusions](#)[References](#)[Tables](#)[Figures](#)[⏪](#)[⏩](#)[◀](#)[▶](#)[Back](#)[Close](#)[Full Screen / Esc](#)[Printer-friendly Version](#)[Interactive Discussion](#)

We can calculate the mass median diameter D_{mass} as:

$$D_{\text{mass}} = \left(\frac{M_m}{\rho} \frac{6}{\pi} \right)^{\frac{1}{3}} \quad (12)$$

where ρ is the density of the dry aerosol (assumed in SAM-TOMAS as 1770 kg m^{-3}). The number-median diameter D_m can be calculated from:

$$D_m = D_{\text{mass}} \exp(-3 \ln^2 \sigma_g) \quad (13)$$

where σ_g is the geometric standard deviation of the aerosol size distribution. We choose a value of 1.4 for σ_g , as this was the median value found for lognormal distributions fitted to the aerosol size distributions of the training data.

3.4 Number of new particles per kg SO_2 emitted

As mentioned in Sect. 2, we have configured the SAM-TOMAS model to use activation-type nucleation for this study. We would therefore expect the source of new particles to increase due to nucleation proportionally with the concentration of H_2SO_4 , which should be roughly proportional to f_{ox} . We would therefore expect a solution that is proportional to f_{ox} and increases with increasing bgSO_2 , but not SO_2emis , as N_{new} is normalized by the SO_2 emissions. We also expect the primary loss mechanism for the newly formed particles to be coagulation with preexisting particles, and this coagulation loss rate is roughly proportional to the condensation sink. We would therefore also expect the solution to exponentially decay with CS (d/v_g). We find the following solution for N_{new} :

$$N_{\text{new}} = 6.939 \times 10^{23} \frac{f_{\text{ox}}^{0.9949} \text{bgSO}_2^{0.2500}}{\text{SO}_2\text{emis}^{0.1280}} \exp \left(-4.417 \text{CS}^{0.1441} \left(\frac{d}{v_g} \right)^{0.1736} \right) \quad (14)$$

where the free parameters for f_{ox} have been fitted to minimize the root-mean-square error in $\log_{10}(N_{\text{new}})$, as was the case for M_m above. Similar to M_m , the NO_xemis scaling

A parameterization of sub-grid particle formation

R. G. Stevens and
J. R. Pierce

Title Page

Abstract

Introduction

Conclusions

References

Tables

Figures

⏪

⏩

◀

▶

Back

Close

Full Screen / Esc

Printer-friendly Version

Interactive Discussion



factor (Eq. 1) used to calculate f_{ox} in N_{new} is several orders of magnitude greater than that used to calculate f_{ox} , as listed in Table 5. This will be discussed further in Sect. 5. We note that the P6 fit value for N_{new} slightly decreases with increasing SO_2 emis. As N_{new} is normalized by the SO_2 emissions, this is consistent with the number of new particles formed in a given plume increasing slightly less than linearly with increasing SO_2 emissions.

3.5 Fraction of sulphate mass that comprises new particles

The mass of new particles per kg SO_2 emitted can be determined from the product of M_m and N_{new} . The product of f_{ox} and f_{new} also yields the mass of SO_2 that ultimately forms new particles per kg SO_2 emitted. We therefore can calculate f_{new} from the other three outputs:

$$f_{\text{new}} = \frac{M_m N_{\text{new}} M_{\text{SO}_2}}{f_{\text{ox}} M_{\text{H}_2\text{SO}_4}} \quad (15)$$

where M_{SO_2} and $M_{\text{H}_2\text{SO}_4}$ are the molar masses of SO_2 and H_2SO_4 , respectively.

However, because the fits for M_m , N_{new} and f_{ox} were performed independently, this equation can yield values for f_{new} greater than 1 under some conditions, which is unphysical. Under such circumstances, we reduce M_m and N_{new} each by a factor of $f_{\text{new}}^{0.5}$ to maintain closure, and limit f_{new} to 1.

4 Comparison of parameterization to full SAM-TOMAS model

We show the correlation coefficient, root-mean-square error, root-mean-square error in the logarithm of the values, and the fraction of the training data cases within a factor of two or ten for each of the outputs in Table 6. We also show the P6 predicted values against the SAM-TOMAS calculated values for f_{ox} , M_m , N_{new} , and f_{new} in Fig. 1. We show the values of M_m , N_{new} , and f_{new} only for cases where nucleation is predicted to occur.

A parameterization of sub-grid particle formation

R. G. Stevens and
J. R. Pierce

Title Page

Abstract

Introduction

Conclusions

References

Tables

Figures

⏪

⏩

◀

▶

Back

Close

Full Screen / Esc

Printer-friendly Version

Interactive Discussion



A parameterization of sub-grid particle formation

R. G. Stevens and
J. R. Pierce

Title Page

Abstract

Introduction

Conclusions

References

Tables

Figures

◀

▶

◀

▶

Back

Close

Full Screen / Esc

Printer-friendly Version

Interactive Discussion

The correlation between the P6 and SAM-TOMAS values of f_{ox} is good ($R = 0.826$). The rms error is comparable to the value of f_{ox} for the majority of the training cases, but this value is dominated by the small number of cases where either the P6 value, the SAM-TOMAS value, or both values of f_{ox} are large. As can be seen in Fig. 1a, a large fraction (69 %) of cases have both P6 and SAM-TOMAS f_{ox} less than 0.02, and the relative error can be large for these cases while the absolute error remains low.

The correlation between the P6 and SAM-TOMAS values of M_m is also good ($R = 0.864$). While the SAM-TOMAS values of M_m span more than five orders of magnitude, we note that the P6 values are within one order of magnitude of the SAM-TOMAS values for nearly all (96.8 %) of the training cases, and for the majority of the cases (59.5 %), they are within a factor of two. Along with the P6 and SAM-TOMAS values of M_m , we also plot the values used by Dentener et al. (2006) and Adams and Seinfeld (2003) for M_m in Fig. 1b. We note that the value of M_m from Dentener et al. (2006) is more than three orders of magnitude larger than the largest value calculated by SAM-TOMAS for the training simulations. The value from Adams and Seinfeld (2003) is within the range of values predicted by SAM-TOMAS, but is more than two orders of magnitude larger than the median value of M_m for the training simulations. There is a large fraction of new-particle-formation cases (40 %) where both P6 and SAM-TOMAS values of M_m do not exceed 2×10^{-22} kg, corresponding to a mass median diameter of less than 6 nm.

While the P6 parameterization does not capture the behaviour of N_{new} as well as it captures the behaviour of f_{ox} and M_m , the P6 values are still within one order of magnitude of the SAM-TOMAS values for most (83.8 %) of the training cases, across which the SAM-TOMAS values vary by more than six orders of magnitude. In addition to the P6 and SAM-TOMAS values of N_{new} , we also plot the values used by Dentener et al. (2006) and Adams and Seinfeld (2003) for N_{new} in Fig. 1c. We note that the value of N_{new} from Dentener et al. (2006) is more than two orders of magnitude smaller than the smallest value calculated by SAM-TOMAS for the training simulations. The value from Adams and Seinfeld (2003) is within the range of values predicted by SAM-

TOMAS, but is nearly one order of magnitude larger than the median value of N_{new} for the training simulations.

As the P6 values of f_{new} are calculated based on f_{ox} , M_m , and N_{new} , instead of being fit directly to the SAM-TOMAS values, we would expect this variable to show the poorest fit to the SAM-TOMAS values. Since f_{ox} and f_{new} are uncorrelated, there will be instances where the value of f_{ox} is small, and hence the relative error in f_{ox} may be high, but the value of f_{new} is not small. Since f_{new} is calculated using f_{ox} , a large relative error in f_{ox} will yield a high relative in f_{new} , and so this means that the relative error in f_{new} can be high, even for larger values of f_{new} (hence the absolute error will also be large). However, the correlation between the P6 and SAM-TOMAS f_{new} values remains good ($R = 0.667$) largely due to resolving the cluster of values near 0 and the cluster near 1 (Fig. 1d). The P6 parameterization correctly predicts low values for f_{new} for the large fraction (56 %) of training cases where the SAM-TOMAS value of f_{new} is less than 0.1, and the P6 value of f_{new} is within 0.1 of the SAM-TOMAS value for 63.3 % of the cases.

5 Sensitivity studies

5.1 Sensitivities to inputs

We show the sensitivities of f_{ox} , M_m , N_{new} , and f_{new} to each of the P6 inputs in Figs. 2, 3, 4, and 5, respectively. Each figure shows green lines for 100 randomly chosen sets of inputs within the ranges of the training data. The black line shows the sensitivity from the set of median values for each input ($\text{SO}_2\text{emis} = 0.1 \text{ kg s}^{-1}$, $\text{NO}_x\text{emis} = 0.05 \text{ kg s}^{-1}$, $d = 50 \text{ km}$, other values shown in Tables 2 and 3). In each panel, one of the input variables is varied while the others are held fixed. We do not show values for M_m , N_{new} , or f_{new} where nucleation is not predicted to occur by the P6 parameterization. Therefore, some lines begin or end in Figs. 3, 4, and 5 as the threshold for nucleation is crossed (Eq. 10)

A parameterization of sub-grid particle formation

R. G. Stevens and
J. R. Pierce

Title Page

Abstract

Introduction

Conclusions

References

Tables

Figures

⏪

⏩

◀

▶

Back

Close

Full Screen / Esc

Printer-friendly Version

Interactive Discussion



A parameterization of sub-grid particle formation

R. G. Stevens and
J. R. Pierce

Title Page

Abstract

Introduction

Conclusions

References

Tables

Figures

⏪

⏩

◀

▶

Back

Close

Full Screen / Esc

Printer-friendly Version

Interactive Discussion

The value of f_{ox} (Fig. 2) is insensitive to SO_2 emis, CS, and bgSO_2 , as one would expect. The value of f_{ox} is also insensitive to NO_x emis. As we note in Sect. 3.1, oxidation generally proceeds much more quickly at the plume edges and in the dilute plume than at the plume centre, so f_{ox} is far more sensitive to bgNO_x than to NO_x emis. As BLH may only affect f_{ox} in the P6 parameterization through the dilution of NO_x emissions, f_{ox} is also insensitive to BLH. The value of f_{ox} is determined by the remaining four inputs. The value of f_{ox} increases with increasing time since emission, and so nearly linearly increases with increasing d and is nearly inversely proportional to v_g . The dependance of f_{ox} on DSWRF and bgNO_x is determined largely by the dependance of OH on these two variables, as parametrized in SAM-TOMAS. The value increases with increasing DSWRF, and there is a peak in f_{ox} at bgNO_x equal to 1 ppb.

The value of M_m is much more sensitive to NO_x emis than to bgNO_x , unlike f_{ox} . Concentrations of SO_2 are highest close to the source, so concentrations of H_2SO_4 (and particle growth rates) may also be highest close to the source, even if SO_2 is being oxidized more slowly. The concentrations of H_2SO_4 close to the source will be more sensitive to NO_x emissions than to background NO_x concentrations, and therefore M_m is also more sensitive to NO_x emis than bgNO_x . This is also reflected in the dependencies of M_m on d and on v_g . The value of f_{ox} is nearly linearly increasing with d , while M_m increases at low values of d but becomes insensitive at higher values. The value of M_m is much less sensitive than f_{ox} to v_g , although this is convoluted by the effect of v_g on M_m through dilution of SO_2 and NO_x emissions, which is also the cause of the slight dependance of M_m on BLH. There is a decrease in M_m with increasing CS, due to the loss in available H_2SO_4 to preexisting particles. We also note that M_m becomes insensitive to SO_2 emis, bgSO_2 and bgNO_x , as well as NO_x emis under some conditions, at small values of each of these inputs. If the background concentrations of NO_x or SO_2 are sufficiently low compared to emissions, in-plume NO_x or SO_2 will be dominated by the emissions, and so further reductions in the background concentrations will not significantly affect M_m . The reverse is also true if the emissions are sufficiently low compared to the background concentrations.

A parameterization of sub-grid particle formation

R. G. Stevens and
J. R. Pierce

Title Page

Abstract

Introduction

Conclusions

References

Tables

Figures

⏪

⏩

◀

▶

Back

Close

Full Screen / Esc

Printer-friendly Version

Interactive Discussion

The value of N_{new} depends on the inputs in a similar manner to M_m . It decreases with increasing CS due to both removal of new particles by coagulation and competition for available H_2SO_4 . It increases with increasing DSWRF. The value of N_{new} is more sensitive to NO_x emis than to bgNO_x . However, N_{new} increases with increasing bgSO_2 , but is generally insensitive to SO_2 emis. Increases in either emissions of SO_2 or the background concentration of SO_2 will increase the available H_2SO_4 , thus increasing new-particle formation, but because N_{new} is defined as the number of new particles normalized by the emissions of SO_2 , changes in the emissions of SO_2 have a small effect on N_{new} . The value of N_{new} also has a complex dependance on v_g and d , either increasing or decreasing with increasing d and decreasing v_g . As the time since emission (d/v_g) increases, N_{new} will increase due to continuing new-particle formation and will decrease due to coagulation scavenging by pre-existing particles. The dependance of N_{new} on d and v_g will depend on the competition between these two processes. We do note, however, that N_{new} tends to asymptote to a single value with increasing d , depending on the values of the other inputs.

Of the four outputs of the P6 parameterization, f_{new} shows the most dramatic changes for small changes in some of the inputs. Specifically, f_{new} is sensitive to small changes for high values of SO_2 emis, high values of bgSO_2 , low values of CS, and, for some combinations of inputs, low values of v_g . The value of f_{new} is less sensitive to the remaining variables, but increases for increasing DSWRF and d , decreases slightly for increasing BLH, and generally decreases with decreasing bgNO_x .

5.2 Sensitivity to number of sources assumed

Often, anthropogenic emissions inventories give emissions of SO_2 and NO_x on a given grid, and not per point source. Figure 6 shows the sensitivity of the P6 parameterization to assumptions about how these emissions are split between sources within the grid box. We used the P6 parameterization to predict f_{ox} , M_m , N_{new} , and f_{new} for 100 different sets of inputs randomly chosen from the range of values tested for each variable, assuming the emissions were split evenly amongst between 1 and 10 point sources.

A parameterization of sub-grid particle formation

R. G. Stevens and
J. R. Pierce

Title Page

Abstract

Introduction

Conclusions

References

Tables

Figures

⏪

⏩

◀

▶

Back

Close

Full Screen / Esc

Printer-friendly Version

Interactive Discussion

variables that are commonly available in global- and regional-scale models. The parameterization predicts the fraction of the emitted SO_2 that is oxidized to form H_2SO_4 , the fraction of that H_2SO_4 that forms new particles, the mean mass per particle of the new particles, and the number of new particles per kg SO_2 emitted. It takes as inputs the source-level SO_2 and NO_x emissions rates, the background aerosol condensation sink, the downward shortwave radiative flux, the mean boundary-layer wind speed, the boundary-layer height, the background SO_2 and NO_x concentrations, and the distance from the source.

In order to create a set of training data for the P6 parameterization, we used the SAM-TOMAS LES/CRM model with online aerosol microphysics, which has been previously shown to well represent the formation and growth of aerosol in coal-fired power-plant plumes. We have shown that the results of the parameterization show good agreement with the results of the SAM-TOMAS model and that the P6 parameterization captures the variability in aerosol formation and growth in sulphur-rich plumes, with correlation coefficients ranging from 0.650 for f_{new} to 0.891 for f_{ox} .

This parameterization will allow for improved representation of sub-grid formation and growth of sulphate aerosol in global- and regional-scale models, allowing for more accurate predictions of aerosol size distributions and improved confidence in studies of aerosol effects on health and climate.

Appendix A

What if one or more of the P6 inputs are not available?

SO_2 emis, NO_x emis: if no estimate of the SO_2 emissions is available, the P6 parameterization can be run assuming a representative distribution of power-plants within the area. This is described in more detail in Sect. 3. If the total NO_x emissions are unknown, the parameterization will assume a SO_2 emis : NO_x emis ratio of 0.419 based on the 2010 CAM data.

grid cell resolution as an approximation for d . We show in our sensitivity studies that for distances greater than 30 km, M_m , N_{new} , and f_{new} are not strongly dependant on d , and f_{ox} is a less than linearly function of d .

5 bgSO₂, bgNO_x: following tables 2.7 of Seinfeld and Pandis (2006), we suggest values of bgNO_x of 10 ppb for urban locations, 1 ppb for rural locations, and 0.05 ppb for remote locations. For bgSO₂ we suggest values of 10 ppb for urban locations, and 0.5 ppb for remote continental conditions, and 0.05 for marine conditions. If no input is given, values of 0.5 ppb and 1 ppb are used for bgSO₂ and bgNO_x.

Supplementary material related to this article is available online at:

10 <http://www.atmos-chem-phys-discuss.net/13/19583/2013/acpd-13-19583-2013-supplement.zip>.

Acknowledgements. We thank the Atlantic Computational Excellence Network (ACENet) for the computational resources used in this study. We also thank the Natural Sciences and Engineering Research Council (NSERC) of Canada for funding.

15 References

- Adams, P. J. and Seinfeld, J. H.: Predicting global aerosol size distributions in general circulation models, *J. Geophys. Res.*, 107, 1–23, doi:10.1029/2001JD001010, 2002.
- Adams, P. J. and Seinfeld, J. H.: Disproportionate impact of particulate emissions on global cloud condensation nuclei concentrations, *Geophys. Res. Lett.*, 30, 1239, doi:10.1029/2002GL016303, 2003.
- 20 Albrecht, B.: Aerosols, cloud microphysics, and fractional cloudiness, *Science*, 245, 1227–1230, 1989.
- Bey, I., Jacob, D. J., Yantosca, R. M., Logan, J. A., Field, B. D., Fiore, A. M., Li, Q., Liu, H. Y., Mickley, L. J., and Schultz, M. G.: Global modeling of tropospheric chemistry with assimilated meteorology: model description and evaluation, *J. Geophys. Res.*, 106, 23073, doi:10.1029/2001JD000807, 2001.
- 25

A parameterization of sub-grid particle formation

R. G. Stevens and
J. R. Pierce

Title Page

Abstract

Introduction

Conclusions

References

Tables

Figures



Back

Close

Full Screen / Esc

Printer-friendly Version

Interactive Discussion



A parameterization of sub-grid particle formation

R. G. Stevens and
J. R. Pierce

Title Page

Abstract

Introduction

Conclusions

References

Tables

Figures

◀

▶

◀

▶

Back

Close

Full Screen / Esc

Printer-friendly Version

Interactive Discussion

- Charlson, R. J., Schwartz, S. E., Hales, J. M., Cess, R. D., Coakley, J. A., Hansen, J. E., and Hofmann, D. J.: Climate forcing by anthropogenic aerosols, *Science*, 255, 423–430, doi:10.1126/science.255.5043.423, 1992.
- Dentener, F., Kinne, S., Bond, T., Boucher, O., Cofala, J., Generoso, S., Ginoux, P., Gong, S., Hoelzemann, J. J., Ito, A., Marelli, L., Penner, J. E., Putaud, J.-P., Textor, C., Schulz, M., van der Werf, G. R., and Wilson, J.: Emissions of primary aerosol and precursor gases in the years 2000 and 1750 prescribed data-sets for AeroCom, *Atmos. Chem. Phys.*, 6, 4321–4344, doi:10.5194/acp-6-4321-2006, 2006.
- Dockery, D., Pope, C., Xu, X., Spengler, J. D., Ware, J. H., Fay, M. E., Ferris, B. G., and Speizer, F. E.: An association between air pollution and mortality in six US cities, *New Engl. J. Med.*, 329, 1753–1759, doi:10.1056/NEJM199312093292401, 1993.
- Dusek, U., Frank, G. P., Hildebrandt, L., Curtius, J., Schneider, J., Walter, S., Chand, D., Drewnick, F., Hings, S., Jung, D., Borrmann, S., and Andreae, M. O.: Size matters more than chemistry for cloud-nucleating ability of aerosol particles, *Science*, 312, 1375–1378, doi:10.1126/science.1125261, 2006.
- Forster, P., Ramaswamy, V., Artaxo, P., Bernsten, T., Betts, R., Fahey, D. W., Haywood, J., Lean, J., Lowe, D. C., Myhre, G., Nganga, J., Prinn, R., Raga, G., Schulz, M., and Dorland, R. V.: Changes in atmospheric constituents and in radiative forcing, in: *Climate Change 2007: The Physical Science Basis, Contribution of Working Group I to the Fourth Assessment Report of the Intergovernmental Panel on Climate Change*, edited by: Miller, H. L., Cambridge University Press, Cambridge, UK and New York, NY, USA, 129–234, 2007.
- Kerminen, V., Lehtinen, K., Anttila, T., and Kulmala, M.: Dynamics of atmospheric nucleation mode particles: a timescale analysis, *Tellus B*, 56, 135–146, 2004.
- Khairoutdinov, M. and Randall, D.: Cloud resolving modeling of the ARM summer 1997 IOP: model formulation, results, uncertainties, and sensitivities, *J. Atmos. Sci.*, 60, 607–626, doi:10.1175/1520-0469(2003)060<0607:CRMOTA>2.CO;2, 2003.
- Kulmala, M. and Kerminen, V.-M.: On the formation and growth of atmospheric nanoparticles, *Atmos. Res.*, 90, 132–150, doi:10.1016/j.atmosres.2008.01.005, 2008.
- Kulmala, M., Lehtinen, K. E. J., and Laaksonen, A.: Cluster activation theory as an explanation of the linear dependence between formation rate of 3nm particles and sulphuric acid concentration, *Atmos. Chem. Phys.*, 6, 787–793, doi:10.5194/acp-6-787-2006, 2006.
- Lee, L. A., Pringle, K. J., Reddington, C. L., Mann, G. W., Stier, P., Spracklen, D. V., Pierce, J. R., and Carslaw, K. S.: The magnitude and causes of uncertainty in global model simulations of

A parameterization of sub-grid particle formationR. G. Stevens and
J. R. Pierce

Title Page

Abstract

Introduction

Conclusions

References

Tables

Figures

◀

▶

◀

▶

Back

Close

Full Screen / Esc

Printer-friendly Version

Interactive Discussion

cloud condensation nuclei, Atmos. Chem. Phys. Discuss., 13, 6295–6378, doi:10.5194/acpd-13-6295-2013, 2013.

Lonsdale, C. R., Stevens, R. G., Brock, C. A., Makar, P. A., Knipping, E. M., and Pierce, J. R.: The effect of coal-fired power-plant SO₂ and NO_x control technologies on aerosol nucleation in the source plumes, Atmos. Chem. Phys., 12, 11519–11531, doi:10.5194/acp-12-11519-2012, 2012.

Luo, G. and Yu, F.: Sensitivity of global cloud condensation nuclei concentrations to primary sulfate emission parameterizations, Atmos. Chem. Phys., 11, 1949–1959, doi:10.5194/acp-11-1949-2011, 2011.

Makkonen, R., Asmi, A., Korhonen, H., Kokkola, H., Järvenoja, S., Räisänen, P., Lehtinen, K. E. J., Laaksonen, A., Kerminen, V.-M., Järvinen, H., Lohmann, U., Bennartz, R., Feichter, J., and Kulmala, M.: Sensitivity of aerosol concentrations and cloud properties to nucleation and secondary organic distribution in ECHAM5-HAM global circulation model, Atmos. Chem. Phys., 9, 1747–1766, doi:10.5194/acp-9-1747-2009, 2009.

Mauldin, R. L., Berndt, T., Sipilä, M., Paasonen, P., Petäjä, T., Kim, S., Kurtén, T., Stratmann, F., Kerminen, V.-M., and Kulmala, M.: A new atmospherically relevant oxidant of sulphur dioxide, Nature, 488, 193–196, doi:10.1038/nature11278, 2012.

Olson, J. R., Crawford, J. H., Chen, G., Brune, W. H., Faloona, I. C., Tan, D., Harder, H., and Martinez, M.: A reevaluation of airborne HO_x observations from NASA field campaigns, J. Geophys. Res., 111, D10301, doi:10.1029/2005JD006617, 2006.

Peters, A., Wichmann, H. E., Tuch, T., Heinrich, J., and Heyder, J.: Respiratory effects are associated with the number of ultrafine particles, Am. J. Resp. Crit. Care, 155, 1376–1383, 1997.

Pierce, J. R. and Adams, P. J.: Global evaluation of CCN formation by direct emission of sea salt and growth of ultrafine sea salt, J. Geophys. Res., 111, D06203, doi:10.1029/2005JD006186, 2006.

Pierce, J. R. and Adams, P. J.: Uncertainty in global CCN concentrations from uncertain aerosol nucleation and primary emission rates, Atmos. Chem. Phys., 9, 1339–1356, doi:10.5194/acp-9-1339-2009, 2009.

Pierce, J. R., Chen, K., and Adams, P. J.: Contribution of primary carbonaceous aerosol to cloud condensation nuclei: processes and uncertainties evaluated with a global aerosol microphysics model, Atmos. Chem. Phys., 7, 5447–5466, doi:10.5194/acp-7-5447-2007, 2007.

A parameterization of sub-grid particle formation

R. G. Stevens and
J. R. Pierce

Title Page

Abstract

Introduction

Conclusions

References

Tables

Figures

⏪

⏩

◀

▶

Back

Close

Full Screen / Esc

Printer-friendly Version

Interactive Discussion

- Pierce, J. R., Evans, M. J., Scott, C. E., D'Andrea, S. D., Farmer, D. K., Swietlicki, E., and Spracklen, D. V.: Weak global sensitivity of cloud condensation nuclei and the aerosol indirect effect to Criegee + SO₂ chemistry, *Atmos. Chem. Phys.*, 13, 3163–3176, doi:10.5194/acp-13-3163-2013, 2013.
- 5 Seinfeld, J. H. and Pandis, S. N.: *Atmospheric Chemistry and Physics: From Air Pollution to Climate Change*, 2nd edn., John Wiley and Sons, Inc., Hoboken, New Jersey, 2006.
- Snow-Kropla, E. J., Pierce, J. R., Westervelt, D. M., and Trivitayanurak, W.: Cosmic rays, aerosol formation and cloud-condensation nuclei: sensitivities to model uncertainties, *Atmos. Chem. Phys.*, 11, 4001–4013, doi:10.5194/acp-11-4001-2011, 2011.
- 10 Spracklen, D. V., Pringle, K. J., Carslaw, K. S., Chipperfield, M. P., and Mann, G. W.: A global off-line model of size-resolved aerosol microphysics: I. Model development and prediction of aerosol properties, *Atmos. Chem. Phys.*, 5, 2227–2252, doi:10.5194/acp-5-2227-2005, 2005.
- Stevens, R. G., Pierce, J. R., Brock, C. A., Reed, M. K., Crawford, J. H., Holloway, J. S., Ryerson, T. B., Huey, L. G., and Nowak, J. B.: Nucleation and growth of sulfate aerosol in coal-fired power plant plumes: sensitivity to background aerosol and meteorology, *Atmos. Chem. Phys.*, 12, 189–206, doi:10.5194/acp-12-189-2012, 2012.
- Trivitayanurak, W., Adams, P. J., Spracklen, D. V., and Carslaw, K. S.: Tropospheric aerosol microphysics simulation with assimilated meteorology: model description and intermodel comparison, *Atmos. Chem. Phys.*, 8, 3149–3168, doi:10.5194/acp-8-3149-2008, 2008.
- 20 Twomey, S.: Pollution and planetary albedo, *Atmos. Environ.*, 8, 1251–1256, doi:10.1016/0004-6981(74)90004-3, 1974.
- United States Environmental Protection Agency: Clean Air Markets: Data and Maps, available at: <http://ampd.epa.gov/ampd/> (last access: March 2013), 2012.
- 25 Wang, M. and Penner, J. E.: Aerosol indirect forcing in a global model with particle nucleation, *Atmos. Chem. Phys.*, 9, 239–260, doi:10.5194/acp-9-239-2009, 2009.
- Yu, F.: Diurnal and seasonal variations of ultrafine particle formation in anthropogenic SO₂ plumes., *Environ. Sci. Technol.*, 44, 2011–2015, doi:10.1021/es903228a, 2010.
- Yu, F. and Luo, G.: Simulation of particle size distribution with a global aerosol model: contribution of nucleation to aerosol and CCN number concentrations, *Atmos. Chem. Phys.*, 9, 7691–7710, doi:10.5194/acp-9-7691-2009, 2009.
- 30

A parameterization of sub-grid particle formation

R. G. Stevens and
J. R. Pierce

Title Page

Abstract

Introduction

Conclusions

References

Tables

Figures

⏪

⏩

◀

▶

Back

Close

Full Screen / Esc

Printer-friendly Version

Interactive Discussion



Table 1. Parameter space used to create training data for the P6 parameterization.

Parameter	Minimum	Maximum
Latitude	30° N	70° N
Longitude	55° W	110° W
Time	1 Jul 2010, 15:00 UTC	28 Jul 2010, 21:00 UTC
Distance from source	5 km	100 km
$\log_{10}(\text{SO}_2\text{emis} [\text{kg s}^{-1}])$	-3	1
$\log_{10}(\text{NO}_x\text{emis} [\text{kg s}^{-1}])$	-3	0.3
Emissions height	60 m	580 m

A parameterization of sub-grid particle formation

R. G. Stevens and
J. R. Pierce

Title Page

Abstract

Introduction

Conclusions

References

Tables

Figures

⏪

⏩

◀

▶

Back

Close

Full Screen / Esc

Printer-friendly Version

Interactive Discussion

Table 2. Outputs from GEOS-Chem-TOMAS used as inputs for SAM-TOMAS. The fully resolved aerosol size distribution from GEOS-Chem-TOMAS was used in SAM-TOMAS, but for conciseness we only tabulate the condensation sink here. Cases where the DSWRF was less than 100 were excluded from this study, because of uncertainties associated with OH production for these conditions.

Parameter	Minimum	Maximum	Median
Condensation sink [s^{-1}]	8.94×10^{-5}	1.46×10^{-2}	1.38×10^{-3}
Background SO_2 [ppb]	1.27×10^{-6}	16.6	0.0707
Background NO_x [ppb]	2.84×10^{-4}	7.93	0.0302
DSWRF [$W m^{-2}$]	100	960	401

A parameterization of sub-grid particle formation

R. G. Stevens and
J. R. Pierce

[Title Page](#)[Abstract](#)[Introduction](#)[Conclusions](#)[References](#)[Tables](#)[Figures](#)[◀](#)[▶](#)[◀](#)[▶](#)[Back](#)[Close](#)[Full Screen / Esc](#)[Printer-friendly Version](#)[Interactive Discussion](#)

Table 3. Minimum, maximum, and median values of the mean boundary-layer wind speeds and the boundary-layer heights for the training data used in this study.

Parameter	Minimum	Maximum	Median
Wind speed [m s^{-1}]	0.178	26.1	5.98
Boundary-layer height [m]	53	2792	434

A parameterization of sub-grid particle formation

R. G. Stevens and
J. R. Pierce

Title Page

Abstract

Introduction

Conclusions

References

Tables

Figures

◀

▶

◀

▶

Back

Close

Full Screen / Esc

Printer-friendly Version

Interactive Discussion

Table 5. Emissions scaling factors used in the P6 parameterization for determining effective SO_2 and NO_x concentrations (Eq. 1 and Eq. 9)

	NO_x emis scaling factor	SO_2 emis scaling factor
In-plume mean concentration	9.595×10^4	1.705×10^4
f_{ox}	1.444×10^{-8}	–
nucleation	4.365×10^5	2.239×10^4
M_m	2.139×10^7	2.605×10^6
N_{new}	1.243×10^6	–

A parameterization of sub-grid particle formation

R. G. Stevens and
J. R. Pierce

Title Page

Abstract

Introduction

Conclusions

References

Tables

Figures

◀

▶

◀

▶

Back

Close

Full Screen / Esc

Printer-friendly Version

Interactive Discussion

Table 6. Quality of fit information for the P6 parameterization predicted outputs and the results of SAM-TOMAS.

	correlation coefficient	rms error	rms log ₁₀ error	fraction within a factor of 2	fraction within a factor of 10
f_{ox}	0.826	0.0190	0.845	50.3 %	77.0 %
M_m	0.891	1.38×10^{-19} kg	0.425	60.0 %	96.7 %
N_{new}	0.670	4.85×10^{18} (kg SO ₂) ⁻¹	0.741	36.2 %	84.6 %
f_{new}	0.650	0.289	1.07	28.6 %	66.8 %

A parameterization of sub-grid particle formation

R. G. Stevens and
J. R. Pierce

Title Page

Abstract

Introduction

Conclusions

References

Tables

Figures



Back

Close

Full Screen / Esc

Printer-friendly Version

Interactive Discussion

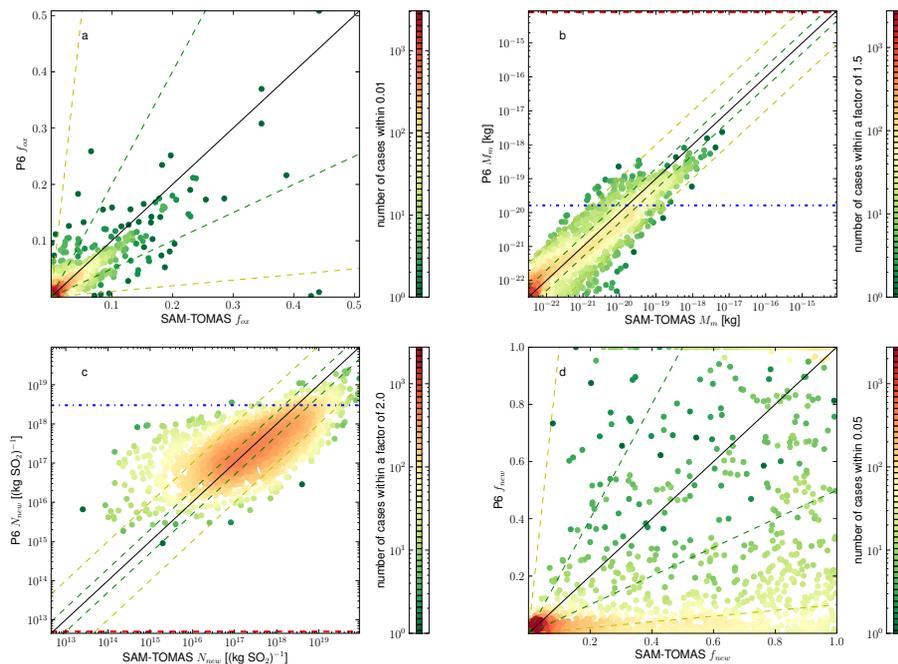


Fig. 1. P6 vs SAM-TOMAS values of f_{ox} , M_m , N_{new} , and f_{new} . Color of points indicates density of cases. The red dashed lines indicate the values of M_m and N_{new} from Dentener et al. (2006), and the blue dashed-dotted line indicate the values of M_m and N_{new} from Adams and Seinfeld (2003). The green and yellow dashed lines indicate where the predicted values are within a factor of two and ten, respectively, of the calculated values.

A parameterization of sub-grid particle formation

R. G. Stevens and J. R. Pierce

Title Page	
Abstract	Introduction
Conclusions	References
Tables	Figures
◀	▶
◀	▶
Back	Close
Full Screen / Esc	
Printer-friendly Version	
Interactive Discussion	

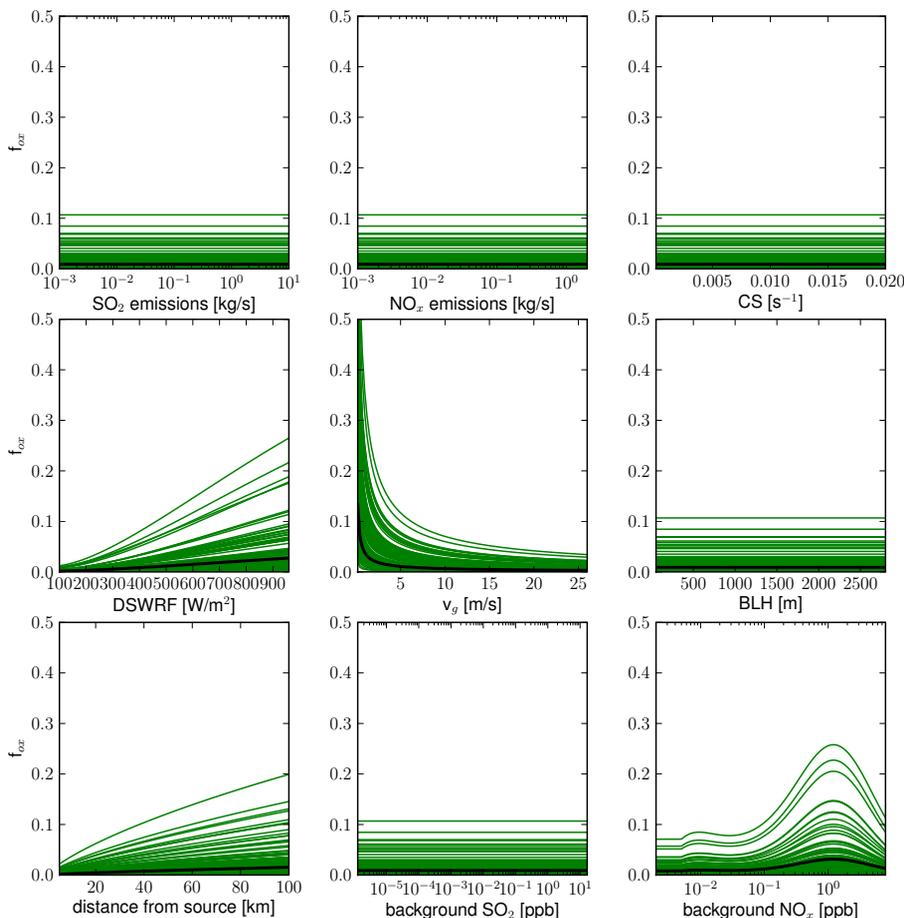


Fig. 2. Sensitivity of f_{ox} to each of the inputs for 100 randomly selected sample inputs. The black line denotes the median value case.



A parameterization of sub-grid particle formation

R. G. Stevens and
J. R. Pierce

Title Page

Abstract

Introduction

Conclusions

References

Tables

Figures

◀

▶

◀

▶

Back

Close

Full Screen / Esc

Printer-friendly Version

Interactive Discussion

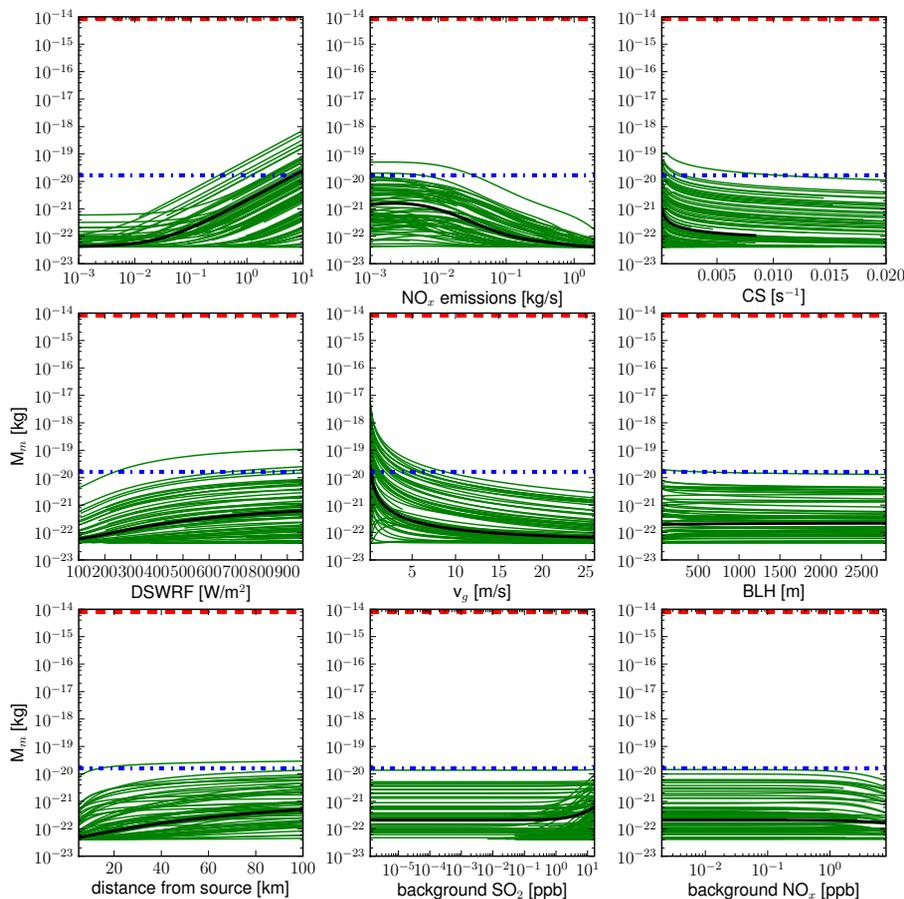


Fig. 3. Sensitivity of M_m to each of the inputs for 100 randomly selected sample inputs. If nucleation is not predicted by the P6 parametrization, no value is shown. The black line denotes the median value case. The red dashed line indicates the value from Dentener et al. (2006), and the blue dashed-dotted line indicates the value from Adams and Seinfeld (2003).

A parameterization of sub-grid particle formation

R. G. Stevens and
J. R. Pierce

Title Page

Abstract

Introduction

Conclusions

References

Tables

Figures

◀

▶

◀

▶

Back

Close

Full Screen / Esc

Printer-friendly Version

Interactive Discussion

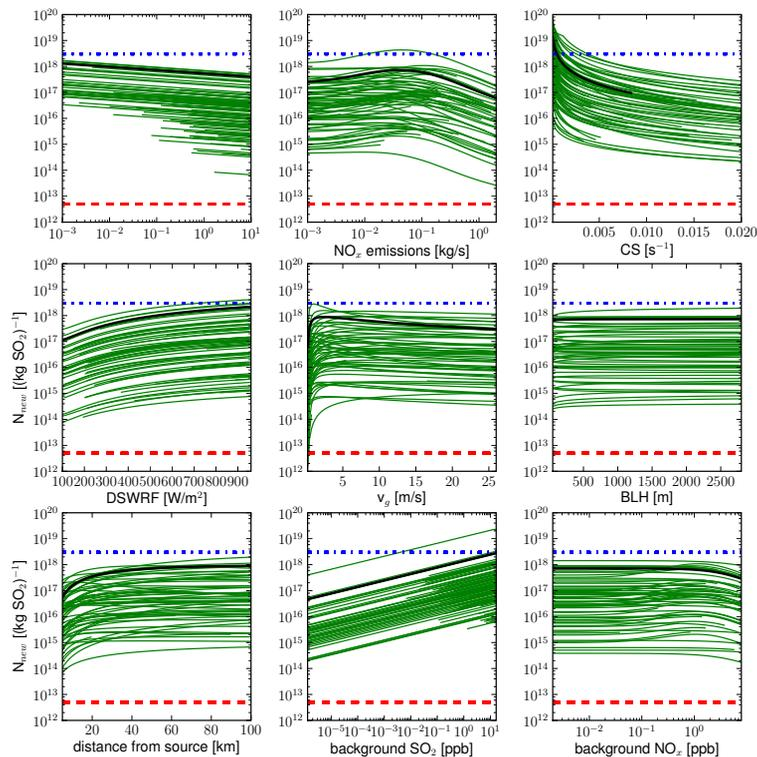


Fig. 4. Sensitivity of N_{new} to each of the inputs for 100 randomly selected sample inputs. If nucleation is not predicted by the P6 parametrization, no value is shown. The black line denotes the median value case. The red dashed line indicates the value from Dentener et al. (2006), and the blue dashed-dotted line indicates the value from Adams and Seinfeld (2003).

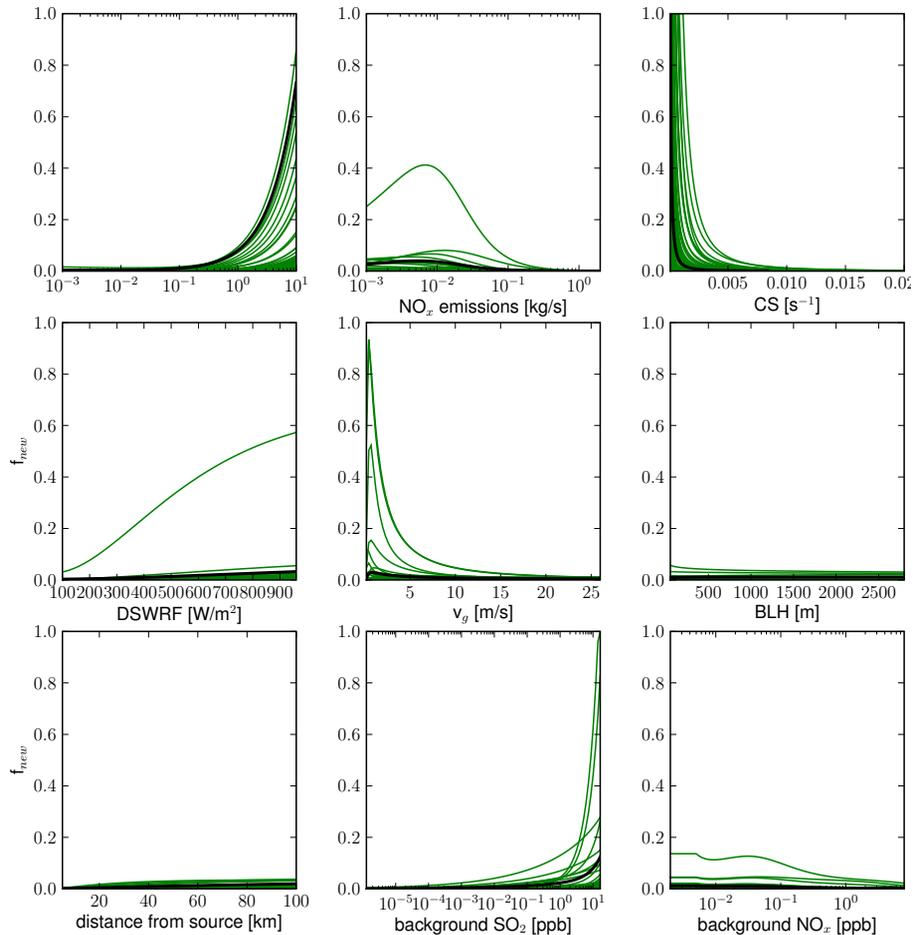


Fig. 5. Sensitivity of f_{new} to each of the inputs for 100 randomly selected sample inputs. If nucleation is not predicted by the P6 parametrization, no value is shown. The black line denotes the median value case.

A parameterization of sub-grid particle formation

R. G. Stevens and
J. R. Pierce

Title Page

Abstract

Introduction

Conclusions

References

Tables

Figures

⏪

⏩

◀

▶

Back

Close

Full Screen / Esc

Printer-friendly Version

Interactive Discussion

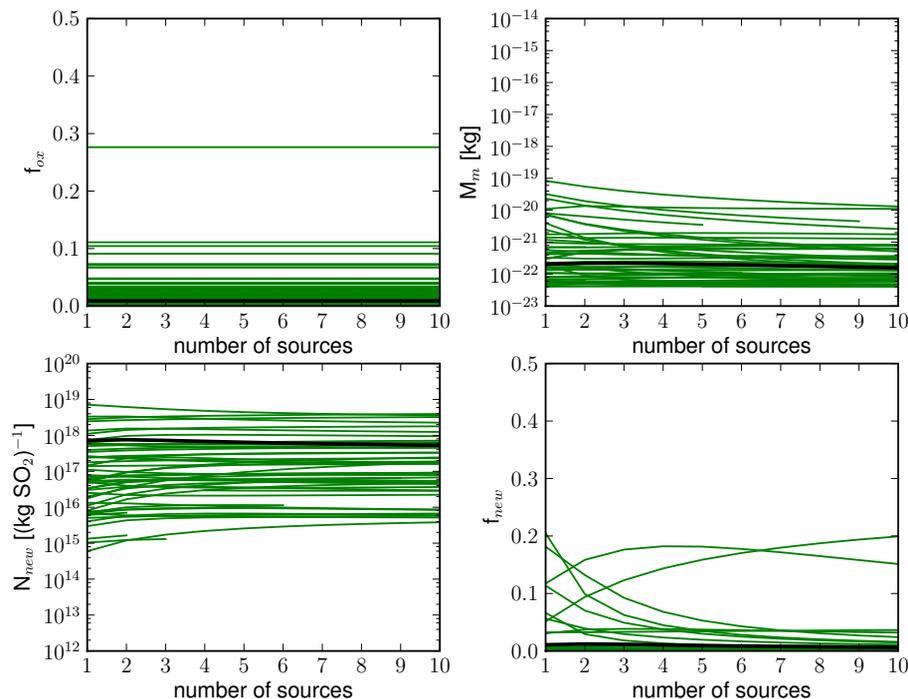


Fig. 6. Sensitivity of f_{ox} , M_m , N_{new} , and f_{new} to the assumed number of emission sources, while keeping total emissions of SO_2 and NO_x constant, for 100 randomly selected sets of inputs. If nucleation is not predicted by the P6 parametrization, no value is shown. The black line in each figure denotes the median value case.